Available online at www.sciencedirect.com

ScienceDirect

journal homepage: www.elsevier.com/locate/issn/15375110

Research Paper

Detecting powdery mildew disease in squash at different stages using UAV-based hyperspectral imaging and artificial intelligence

Jaafar Abdulridha [a,**], *Yiannis Ampatzidis* [a,*], *Pamela Roberts* [b], *Sri Charan Kakarla* [a]

[a] *Agricultural and Biological Engineering Department, Southwest Florida Research and Education Center, University of Florida, 2685 FL-29, Immokalee, 34142, Florida, USA*

[b] *Plant Pathology Department, Southwest Florida Research and Education Center, University of Florida, 2685 FL-29, Immokalee, 34142, Florida, USA*

ARTICLE INFO

Article history:
Received 17 December 2019
Received in revised form
18 June 2020
Accepted 1 July 2020

Keywords:
Disease detection
Vegetation indices
Remote sensing
Machine learning

In this study hyperspectral imaging (380–1020 nm) and machine learning were utilised to develop a technique for detecting different disease development stages (asymptomatic, early, intermediate, and late disease stage) of powdery mildew (PM) in squash. Data were collected in the laboratory as well as in the field using an unmanned aerial vehicle (UAV). Radial basis function (RBF) was used to discriminate between healthy and diseased plants, and to classify the severity level (disease stage) of a plant; the most significant bands to differentiate between healthy and different stages of disease development were selected (388 nm, 591 nm, 646 nm, 975 nm, and 1012 nm). Furthermore, 29 spectral vegetation indices (VIs) were tested and evaluated for their ability to detect and classify healthy and PM-infected plants; the M value was used to evaluate the VIs. The water index (WI) and the photochemical reflectance index (PRI) were able to accurately detect and classify PM in asymptomatic, early, and late development stages under laboratory conditions. Under field conditions (UAV-based), the spectral ratio of 761 (SR761) accurately detected PM in early stages, and the chlorophyll index green (CI green), the normalised difference of 750/705 (ND 750/705), the green normalised difference vegetation index (GNDVI), and the spectral ratio of 850 (SR850) in late stages. The classification results, by using RBF, in laboratory conditions for the asymptomatic and late stage was 82% and 99% respectively, while in field conditions it was 89% and 96% in early and late disease development stages, respectively.

* *Corresponding author.*
** *Corresponding author.*
E-mail addresses: ftash@ufl.edu (J. Abdulridha), i.ampatzidis@ufl.edu (Y. Ampatzidis), pdr@ufl.edu (P. Roberts).
https://doi.org/10.1016/j.biosystemseng.2020.07.001

1. Introduction

Summer squash (*Cucurbita pepo*) is an important vegetable crop and economically valuable in many areas. However, squash and other members of Cucurbitaceae are highly susceptible to the powdery mildew disease caused by the fungus *Podosphaera xanthii* (Cohen, Hanan, & Paris, 2003). Powdery mildew (PM) is a common disease on squash in the United States and throughout the world. The PM disease can decrease yield potential and reduce fruit quality if it is not controlled during the early infection phases (McGrath, Fox, & Menasha, 2009). The main symptom of PM consists of white powdery spots or patches, usually on the leaves. Diagnosing PM in early infection stages is problematic, due to the presence of PM symptoms on lower, more mature leaves, which are often covered by other leaves in the plant's canopy that makes it difficult to detect. It is crucial to identify PM early, since the disease spreads rapidly and the lesions increase in size, developing a dusty white or gray coating. The ideal environment for PM to infect is humid weather, high density planting and shade, but dryer conditions without rain or leaf wetness favor inoculum production and spread (Reuveni, 1974, pp. 25–33). The PM causes leaves, stems, and flowers to become distorted and stunted. Spores are readily wind-dispersed over long distances (Reuveni, 1974, pp. 25–33).

Early disease detection is necessary for optimal PM management to control and prevent the spread of the disease throughout the field. In addition to early detection, two main issues have to be addressed for an efficient PM management: i) determining the progression of the disease, and ii) determining the location and severity of the disease of the outbreak. Frequent spray applications with large amounts of chemicals such as fungicides contribute to the accumulation of chemical waste in soil and water, increase environmental pollution and contamination of edible products (Itoh, 2014; Lapushkina, Andreeva, & Slynko, 2002). Frequent dosages of some pesticides would lead to selection and an increase in pesticide resistance in pest and pathogen populations. Spraying large amounts of pesticides will damage the ecosystem and potentially harm global health of plants, animals, and human beings (Brisbois, Harris, & Spiegel, 2018; Spurgeon et al., 2016). Smart and precision agriculture technologies could provide a long term solution by early detecting pest and plant diseases and by developing target-based spraying technologies (Partel, Kakarla, & Ampatzidis, 2019). For example, Faical et al. (2017) developed a dynamic computer-based method that was able to autonomously adjust the flying rules of a spraying unmanned aerial vehicle (UAV) based on changes in weather conditions for more accurate pesticide deposition on the target fields. Xiongkui, Aijun, and Jianli (2011) developed a precision orchard sprayer utilising infrared sensing and electrostatic techniques that was able to save more than 50%–75% of pesticides. For the better utilisation of precision spraying technologies, an early disease detection system is needed. Detecting the disease at an early stage allows growers to take appropriate management steps (i.e. fungicide application), mitigate losses due to the disease, and increase profitability. Visible and near infrared (NIR) spectroscopy is one of the most commonly used nondestructive methods for detecting plant diseases in laboratory and field (Ampatzidis, De Bellis, & Luvisi, 2017; Luvisi, Ampatzidis, & De Bellis, 2016). Xu, Ying, Fu, and Zhu (2007) monitored five disease stages of leafminer damage in tomato leaves by using NIR spectroscopy (800–2500 nm) and found that the most sensitive bands were located at 1450 and 1900 nm. Al-Ahmadi et al. (2018) utilised a NIR technique (900–2400 nm) to monitor soybean plants, which were treated with toxins produced by the charcoal rot pathogen. The results were promising in developing tools to screen soybean varieties tolerant to this disease and for detecting other abiotic factors. Couture et al. (2018) developed a technique to identify the potato virus Y (PVY) in different potato varieties and to monitor the physiological effect of the virus in potato plants. Atanassova, Nikolov, Valchev, and Stoyka Yorgov (2019) used a spectrometer (USB 4000, Ocean Optics, Largo, Florida, USA) (450–1100 nm) to measure the spectral reflectance of cucumber leaves infected with powdery mildew at 3, 5, 7, 9, 11 and 13 days after infection. Several spectral vegetation indices (VIs) (e.g., normalised difference vegetation index, red edge index, photochemical reflectance index, water band index, carotenoid reflectance index) were applied successfully to differentiate between infected plants and healthy plants. Abdulridha, Ehsani, and de Castro (2016) utilised a spectroradiometric hyperspectral device (350–2500 nm) to detect laurel wilt disease in avocados. Abdulridha, Ehsani, Abd-Elrahman, and Ampatzidis (2019c) were able to select the best wavelengths to detect and differentiate laurel wilt and phytophthora root rot, two diseases that cause similar symptoms in early stages. Salinity damage to plants, nitrogen and iron deficiencies in crops were also detected. Several neural network classification methods were applied (multilayer perceptron, radial basis function, tree decision, and stepwise discriminant analysis) and the classification rate between healthy and non-healthy plants was more than 90%.

Recently, UAV-based spectral techniques have been utilised for high throughput plant phenotyping (Ampatzidis & Partel, 2019; Ampatzidis, Partel, & Costa, 2020) and disease detection (Abdulridha, Ampatzidis, Kakarla, & Roberts, 2019a; Hariharan, Fuller, Ampatzidis, Abdulridha, & Lerwill, 2019) in specialty crops. In-field spectral measurements are affected by weather and light conditions (among other factors), in contrast to well-controlled laboratory conditions. Johansen et al. (2019) utilised UAVs to investigate the response of wild tomato plants in relation to salt stress for use in breeding programs to improve salt tolerance in tomato. Martinelli et al. (2015) concluded that UAV-based multispectral or hyperspectral techniques can be used for a more sustainable production system, avoiding expensive use of agrochemicals in yield protection. Tripodi, Massa, Venezia, and Cardi (2018) investigated the benefits of using an UAV-based imaging system to increase the ability of collecting and analysing large set of data in the field in order to precisely evaluate plant phenotypes.

Any disease or stress that affect a plant's chlorophyll concentration, water content, and damage the plant cells would affect the spectral reflectance ratio, and thus, will affect VIs value as well (Semeraro et al., 2019; Zheng et al., 2019). Therefore, it is expected that the values of specific VIs will vary based on disease severity. Vegetation indices combined with image analysis and machine learning could detect

variations in vegetation coverage. Abdulridha, Batuman, and Ampatzidis (2019b) utilised VIs and UAV-based hyperspectral imaging to detect citrus canker and differentiate between healthy and non-healthy citrus trees. The water index (WI) and the modified chlorophyll absorption in reflectance index (ARI and TCARI 1) accurately detected canker to a great extent in laboratory and in orchard conditions, respectively. Candiago, Remondino, De Giglio, Dubbini, and Gattelli (2015) analysed spectral reflectance of vineyards and tomato crops using a UAV-based multispectral camera to estimate the normalised difference vegetation index (NDVI), the green normalised difference vegetation index (GNDVI), and the soil adjusted vegetation index (SAVI) in order to evaluate the vegetation vigor for each crop. For accurate disease detection, it is critical to identify the most significant wavelengths that can be used to not only detect but also distinguish the disease (and its stages) from other diseases and abiotic factors.

The aim of this study was to: i) detect PM on squash plants in the laboratory and in the field (UAV-based) using hyperspectral imaging; ii) monitor plants before detection of PM and after natural infection in both environments (laboratory and field); and iii) obtain the most significant wavelengths and VIs for disease detection and classification.

2. Materials and methods

2.1. Squash plants preparation and inoculation

The experiments were conducted at the Southwest Florida Research and Education Center in Immokalee, FL, USA. Guidelines established by the University of Florida/IFAS were followed for land preparation, fertility, irrigation, weed management, and insect control. Beds were 0.81 m wide with 3.66 m centers covered with black polyethylene film. Yellow crookneck squash seeds were direct seeded on 9 March 2019 into the soil (Immokalee fine sand) in a complete randomised block treatment design with four replicates. Each plot consisted of ten plants spaced 0.91 m apart within an 8.23 m row with 3.05 m between each plot. The plants were infected naturally by PM. Plants were sprayed with fungicides containing active ingredients specific only to oomycetes to control downy mildew and insecticides to control insect pests. Initial detection of powdery mildew was performed with a microscope in the lab to confirm powdery mildew infection on plants in the field. Disease progress was monitored over time throughout the field trial (data not shown) from low disease severity (disease severity is defined as the percentage of symptomatic plant tissue) to high severity with the scale ranging from 0 to 100%.

2.2. Data collection

Squash leaves were collected prior to detection of any symptoms of PM. For laboratory measurements, 10 leaves were regularly collected to monitor the development of the disease after the detection of powdery mildew infection on plants (on April 8, 12, 15, 17, 19, 22, May 1 2019) (Fig. 1a, b and c, and Table 1). UAV imagery was collected on four dates (the first flight took place before the manifestation of the symptoms on April 8th, the second after the first onset on April 15th, the third on April 22nd and the last on May 1st) (Fig. 1d, e and f, and Table 1). The first leaf collection did not show any symptoms, and then the disease severity gradually increased over time.

2.3. Spectral data processing under laboratory conditions

Spectral data were collected using a benchtop hyperspectral imaging system, Pika L 2.4 (Resonon Inc., Bozeman MT, USA) (Fig. 2). The Pika L 2.4 was equipped with a 23 mm lens which has a spectral range of 380–1030 nm, 281 spectral channels, 15.3° field of view and a spectral resolution of 2.1 nm. The same hyperspectral camera was utilised in laboratory and field conditions after changing lenses, which covered the same spectral range. Resonon's hyperspectral imagers (RHI), known as push-broom imagers, are line-scan imagers. The system is made up of a linear stage assembly, which is shifted by a stage motor. Controlled broadband halogen lighting bulbs were set up above the linear stage to produce ideal situations for carrying out the spectral scans. The hyperspectral imaging system was arranged in a way that the lens' distance from the linear stage was 0.5 m. The lights were positioned at the same level as the lens on a parallel plane. All scans were performed using the Spectronon Pro (Resonon Inc., Bozeman MT, USA) software, which was connected to the camera system using a USB cable. Before performing the scans of the leaves, dark current noise was removed using the software. Then, the camera was calibrated by using a white tile (reflectance reference), provided by the manufacturer, placed under the same conditions as used for performing scans. The selection of the regions of interest (RoIs) (Fig. 1a, b & c) was done manually and arbitrarily by picking six spectral scan regions each from 10 leaves to prevent the occurrence of any bias. The total spectral scans (RoIs) selected for each disease stage was 60. RoIs were selected in such a way that they included both the affected and unaffected areas of leaf tissue. The pixel number of each spectral scan selected was between 800 and 900 pixels. The average of 60 spectral scans was used to form an overall spectral scan signature curve for each disease stage. The Spectronon Pro software, which is a post-processing data analysis software, was used to analyse the spectral data of each leaf scan. Several areas containing the symptomatic and non-symptomatic regions on the leaves were selected using the selection tool and the spectrum was generated. For the healthy and asymptomatic stages, several random spots on leaves were selected, and the average of spectral reflectance was calculated and used to form the spectral signature curves.

2.4. UAV spectral data processing in field conditions

The hyperspectral data in field conditions were collected by using an UAV (Matrice 600 Pro, Hexacopter, DJI Inc., Shenzen, China). The UAV-based imaging system included (Fig. 3): (i) a Resonon Pika L 2.4 hyperspectral camera; (ii) a visible-NIR (V-NIR) objective lenses for the Pika L camera with a focal length of 17 mm, field of view (FOV) of 17.6° and an instantaneous field of view (IFOV) of 0.71 mrad; (iii) a Global Navigation Satellite System (GNSS) (Tallysman 33-2710NM-00–3000, Tallysman Wireless Inc., Ontario, Canada)/Inertial Measurement

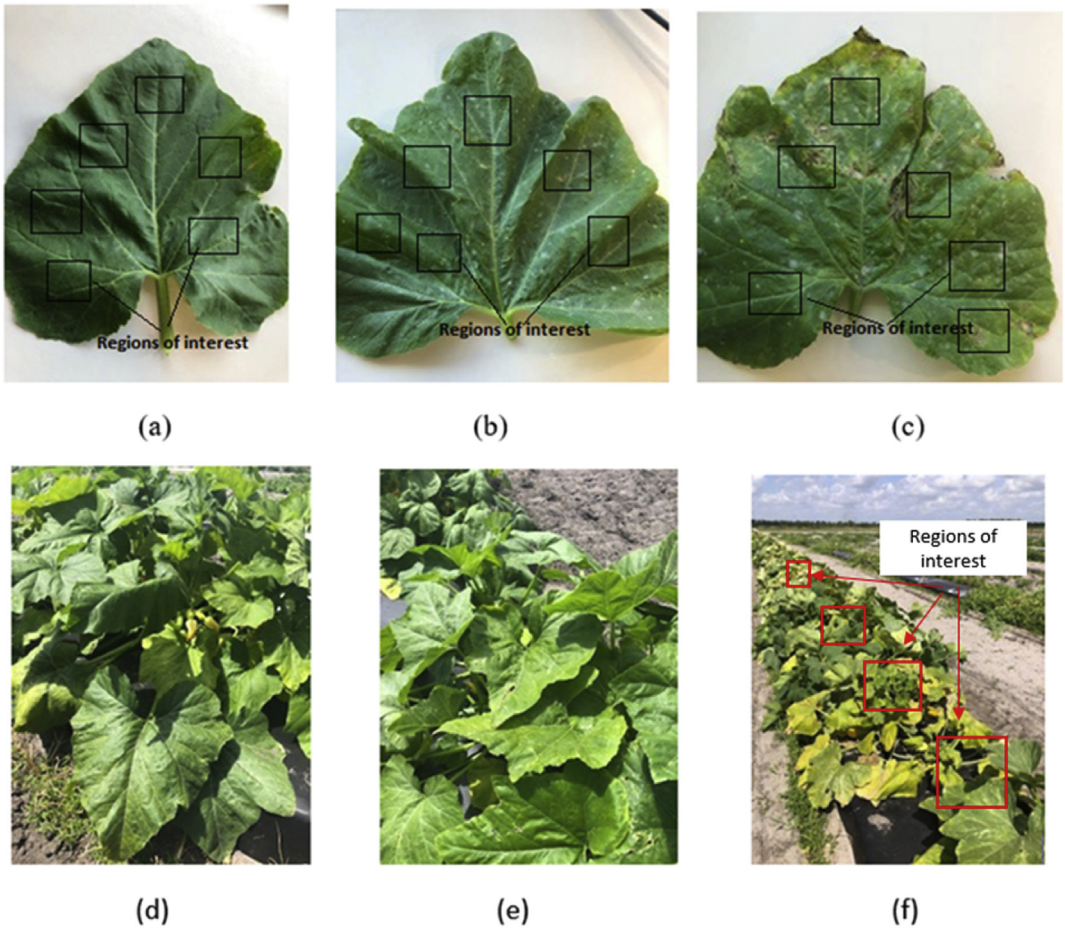

Fig. 1 – Squash plants in different development stages of the powdery mildew disease. The indoor pictures with regions of interest are: a) healthy leaf (prior to any disease detection in field), b) early symptoms (low disease severity), and c) late stage (high disease severity). Outdoor data collection in different disease development stages are d) asymptomatic plants, e) initial symptomatic stage (low disease severity), and f) the late PM symptomatic stage (high disease severity).

Table 1 – Hyperspectral data collection schedule for squash plants in the laboratory and field conditions.

Plant status and disease progress	Category	Collection date	Spectral collection- lab	Spectral collection-UAV
Healthy plant	H	April 8, 2019	√	√
Asymptomatic disease stage	PM1	April 12, 2019	√	
Early symptoms/low disease severity	PM2	April 15, 2019	√	√
Intermediate development stage	PM3	April 17, 2019	√	
Intermediate development stage	PM4	April 19, 2019	√	
Late development disease stage	PM5	April 22, 2019	√	√
Very late development disease stage/high disease severity	PM6	May 1, 2019	√	√

Unit (IMU) (Ellipse N, SGB Systems S.A.S., France) flight control system for multi-rotor aircraft to record sensor position and orientation, and (iv) a Resonon hyperspectral data analysis software (Spectronon Pro, Resonon, Bozeman, MT, USA) which is capable of rectifying the GPS/IMU data using a georectification plugin. The data was collected at 30 m above the ground and at a speed rate of 1.5 m s^{-1}. In the produced map, the pixel size is a function of the working distance (distance between the camera lens and the scanning stage/field) and FOV. This value varies according to the flight parameters. In this study, it was around 35 mm $pixel^{-1}$. Gary tarp at 36% band average reflectivity level (Group VIII Technologies, Provo, Utah, USA) was utilised to correct the data reflectance from radiance. Radiometric calibration was performed by using a calibrated integrating sphere. The manufacturer took 100 lines of hyperspectral data and built a radiometric calibration file that contains a lookup table with all combinations of integration times and framerates. This data was used to convert raw camera data (digital number) to physical units of radiance in micro flicks. The Pika L 2.4 camera is a "pushbroom" or line-scan type imager that produces a 2-D image, where every pixel in the image contains a

Fig. 2 – Laboratory spectral measurements of squash leaves using a benchtop hyperspectral imaging system.

continuous reflectance spectrum. The RoIs were handpicked for each plant, and several spectral scans were done to cover the entire canopy. Each RoI contained four pixels, and four RoIs were selected for each plant. The total sample size for each disease development stage was 20 plants (Fig. 3b). The RoIs were then transferred as a text file and processed using the SPSS software (SPSS 13.0, Inc., Chicago; Microsoft Corp., Redmond, WA).

2.5. *Vegetation indices (VIs)*

The purpose of using VIs in this study is to evaluate their capability on detecting and classifying PM-infected squash plants. In this study, 29 VIs (Table 2) were selected based on their ability to detect differences in plant's concentration of chlorophyll, plant water content, and leaf cell structure. These factors are affected by PM disease (and its severity), and hence the main purpose of this study is to detect the progression of the PM, the proposed VIs could be able to detect these changes and the PM development stages of low to high disease severity progression.

2.6. *Data analysis*

The M value was used to evaluate the selected VIs; the M value divides the difference of mean of two categories (healthy and infected plants) by the sum of the standard deviation (σ) of the two categories (equation (1)).

$$Mvalue = \frac{(Mean_{Healthy} - Mean_{Infected})}{(\sigma_{Healthy} + \sigma_{Infected})} \quad (1)$$

There were six disease stages in the laboratory setting, and the M value was calculated to differentiate the results between each individual stage. The M value is generally higher when the standard deviation is low, which leads to narrowing the histogram of spectral reflectance, which leads to less overlap (Kaufman & Remer, 1994). The M value is considered as a significant discriminant between different VIs. As the value of M value increases, less overlap and better reparability is observed. Furthermore, the Tukey's HSD test ($\alpha = 0.01$) was

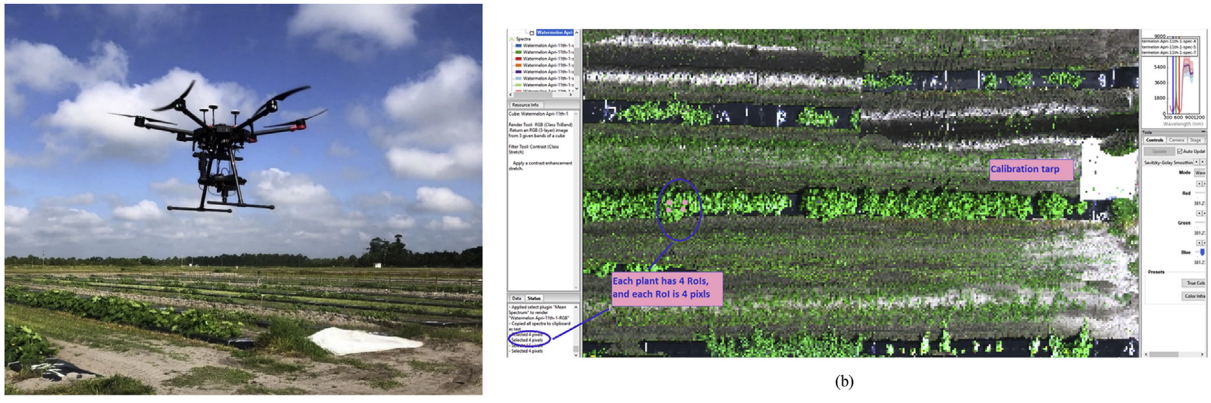

(a) (b)

Fig. 3 – a) An UAV-based imaging data collection with a hyperspectral Resonon camera of a squash field at the Southwest Florida Research and Education Center, and b) aerial image showing the regions of interest were selected and calibration tarp.

Table 2 – Vegetation indices studied in this work to detect PM.

VIs	Equations	References
Ratio Analysis of reflectance Spectral Chlorophyll-a (RARSa)	$RARSa = \frac{R675}{R700}$	Chappelle, Kim, and McMurtrey (1992)
Ratio Analysis of reflectance Spectral Chlorophyll b (RARSb)	$RARSb = \frac{R675}{(R700 \times R650)}$	Chappelle et al. (1992)
Ratio analysis of reflectance spectra (RARSc)	$RARSc = \frac{R760}{R500}$	Chappelle et al. (1992)
Pigment specific simple ratio (PSSRa)	$PSSRa = \frac{R800}{R680}$	Blackburn (1998)
Normalised difference vegetation index 780 (NDVI 780)	$NDVI780 = \frac{R780 - R670}{R780 + R670}$	Raun et al. (2001)
Green NDVI (GNDVI)	$GNDVI = \frac{(NIR850 - G580)}{(NIR850 + G580)}$	Gitelson and Merzlyak (1996)
Photochemical Reflectance Index (PRI)	$PRI = \frac{(R532 - R570)}{(R531 + R570)}$	Penuelas, Pinol, Ogaya, and Filella (1997b)
Simple Ratio Index (SR900)	$SR900 = \frac{R900}{R680}$	Jordan (1969)
Water Index (WI)	$WI = \frac{R900}{R970}$	Penuelas, Llusia, Pinol, and Filella (1997a)
Structure Insensitive Pigment Index (SIPI)	$SIPI = \frac{(R840 - R450)}{(R840 - R670)}$	Penuelas, Baret, and Filella (1995)
Normalised phaeophytinization index (NPQI)	$NPQI = \frac{(R415 - R435)}{(R415 + R435)}$	Barnes, Balaguer, Manrique, Elvira, and Davison (1992)
Normalised difference vegetation index (NDVI 760)	$NDVI761 = \frac{(R761 - R450)}{(R761 - R450)}$	Raun et al. (2001)
Normalised difference vegetation index 850 (NDVI 850)	$NDVI850 = \frac{(R850 - R651)}{(R850 + R651)}$	Raun et al. (2001)
Simple Ratio Index (SR 760)	$SR761 = \frac{R761}{R650}$	Jordan (1969)
Simple Ratio Index (SR 850)	$SR850 = \frac{(R850)}{(R650)}$	Jordan (1969)
Triangle Vegetation Index (TVI)	$TVI = 0.5[120^{a}(R750\text{-}R550)\text{-}200(R670\text{-}R550)]$	Broge and Leblanc (2001)
Modified Triangular Vegetation Index1 (MTVI 1)	$MTVI\ 1 = 1.2[1.2^{a}(R800\text{-}R550)\text{-}2.5(R670\text{-}R550)]$	Haboudane, Miller, Pattey, Zarco-Tejada, and Strachan (2004)
Modified Triangular Vegetation Index2 (MTVI 2)	$MTVI2 = 1.5\frac{[1.2(R760 - R580) - 2.5(R650 - R580)]}{SQ}$	Haboudane et al. (2004)
Renormalised Difference Vegetation Index (RDVI)	$RDVI = \frac{(R760 - R650)}{(R760 + R650)^{0.5}}$	Roujean and Breon (1995)
Red-Edge Vegetation Stress Index 1 (RVS 1)	$RVSI1 = \frac{(R650 + Edge750)}{2} - Edge733$	Merton (1998)
Structure Insensitive Pigment Index (SIPI)	$SIPI = \frac{(R840 - R450)}{(R840 - R670)}$	Penuelas et al. (1995)
Transform chlorophyll absorption in reflectance index (TCARI)	$TCARI = 3[(R740\text{-}R651)\text{-}0.2(R740\text{-}R581)\ (R740/R651)]$	Haboudane, Miller, Tremblay, Zarco-Tejada, and Dextraze (2002)
Photochemical Reflectance Index (PRI)	$PRI = \frac{(R531 - R570)}{(R531 + R570)}$	Gamon, Penuelas, and Field (1992)
Normalise difference of 750/705	$ND750/705\frac{(R750 - R705)}{(R750 + R705)}$	Raun et al. (2001)
Modified Chlorophyll Absorption in Reflectance Index (mCARI 1)	$mCARI\ 1 = 1.2[(2.5^{a}(R761 - R651)\text{-}1.3(R761 - R581)]$	Haboudane et al. (2004)
Anthocyanin Reflectance Index (ARI)	$ARI = \left(\frac{1}{R550}\right) - \left(\frac{1}{R700}\right)$	Gitelson, Merzlyak, and Chivkunova (2001)

Table 2 – (continued)

VIs	Equations	References
Chlorophyll Index (CI green)	$CI = \left(\frac{R840}{R570}\right) - 1$	Gitelson, Gritz, and Merzlyak (2003)
Chlorophyll-Index Rededge (*CIrededge*	$CIrededge = \left(\frac{R780}{R705}\right) - 1$	Gitelson et al. (2003)
Chlorophyll vegetation index	$CVI = R840\left(\frac{R760}{R550^2}\right)$	Vincini, Frazzi, and D'Alessio (2007)

[a] Blue range: 430–450 nm, green range: 520–550 nm, red range: 620–670 nm, red edge: 730–780, and NIR: 830–850 nm.

used to analyses and evaluate all VIs using the SPSS software.The sensitivity value was another parameter that we utilised in this study to evaluate the VIs. The sensitivity value was calculated as the mean reflectance value of diseased leaves divided by the mean reflectance value of healthy leaves (at each wavelength).

2.7. *Radial basis function network (RBF)*

A radial basis function (RBF) network is a type of neural network. It makes use of supervised machine learning to work as a non-linear classifier. In contrast to simple linear classifiers that work on lower-dimensional vectors, non-linear classifiers use advanced functions to go further deep into the analysis. An RBF performs classification by measuring the input's similarity to examples from the training set. Each RBF neuron stores a "prototype", which is just one of the examples from the training set. When we want to classify a new input, each neuron computes the Euclidean distance between the input and its prototype. RBF network uses radial basis functions as its activation functions. The activation functions of artificial neurons drive outputs that can be represented in different ways to show how the network classifies data points. RBF network consists of input layers, hidden layers and output layers similar to other types of neural networks. It often includes some type of non-linear activation function. Gradient descent is used for the training of output weights. RBF is generally considered a relatively intuitive approach and a better way to address specialised machine learning problems. In this study, the dataset (spectral signatures) were divided in: 70% training, 20% testing, and 10% holdout for validation of the RBF neural network (Delnavaz & Zangooei, 2016).

3. Results and discussion

3.1. *Spectral reflectance and classification analysis of PM-infected squash in laboratory conditions*

Leaves were collected every 3–4 days, based on the progress of PM disease (Table 1), to measure their spectral reflectance under laboratory conditions. It was difficult to visually detect the disease in the surveyed plants during the first two days because the infected leaves were hidden beneath the non-infected leaves. White powdery fungal growth develops on both leaf surfaces, petioles, and stems, and usually, it develops first on lower, mature leaves. Since, the infected leaves were in the lower part of the plant canopy beneath younger leaves, these factors make it difficult for the detection and collection of PM-infected leaves. Yellow spots may form on upper leaf surfaces opposite powdery mildew colonies (McGrath, 1997). The spectral reflectance of leaves across time varied depending on the disease symptoms. Figure 4 shows that the spectral reflectance of leaves was increased in the green and red range gradually as the disease progressed. The increase of symptoms increased the spectral reflectance of leaves to a very high level as in the late stage of PM disease. It can be observed that the spectral reflectance of leaves in the red range has a different shape when compared between late disease stage and healthy or early disease stage. The most significant bands were in the visible range, as the highest spectral reflectance value was recorded in the red range at 630 nm for the late stage. The difference in sensitivity values between asymptomatic and very early stage progress of PM was noticeable at the range of 500–730 nm (Fig. 5). The most significant difference in sensitivity values can be noticed between the asymptomatic stage and the very late stage, with a highest at 394 nm (Fig. 5). In initial PM stages, the RBF classification rate achieved 82% accuracy, and it kept increasing

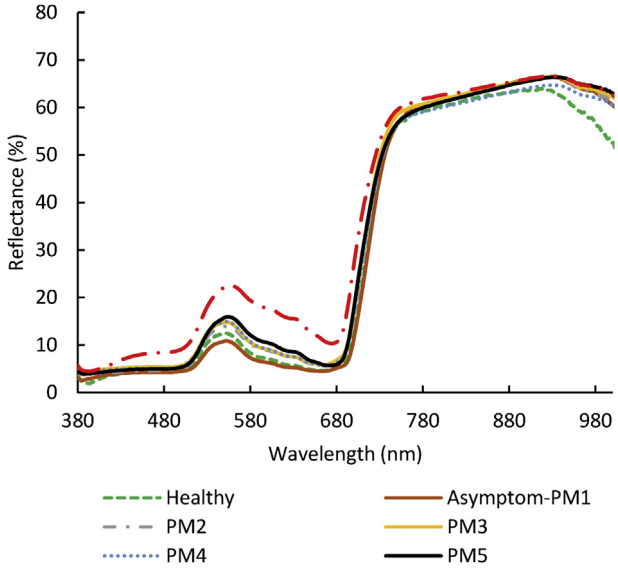

Fig. 4 – Spectral reflectance signatures of healthy squash plants and PM-infected plants in different disease development stages (asymptomatic, early - late stages), obtained under laboratory conditions.

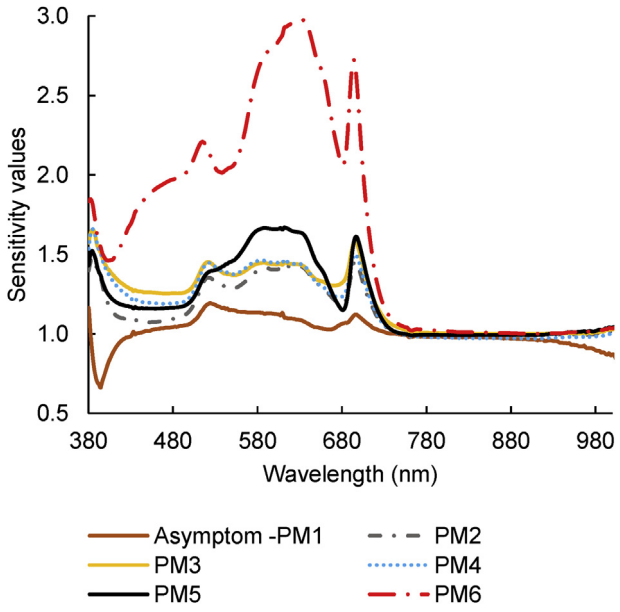

Fig. 5 – Sensitivity values of PM-infected squash plants under laboratory conditions.

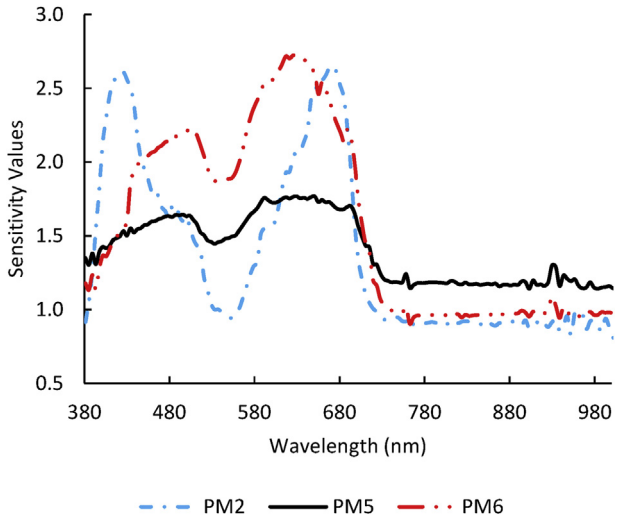

Fig. 7 – Sensitivity values of PM-infected squash plants; spectral data were collected using the UAV-based technique.

gradually to reach 99% in the late stages (Fig. 8a). The best bands, where the most significant difference could be observed, were selected between 966 nm and 989 nm for PM1, PM2, PM3 and PM4 stages. Pairwise comparisons between the healthy and each one of the PM stages using Tukey's HSD (Honestly Significant Difference with $\alpha = 0.01$) test indicated that all wavebands presented in Table 3 can be used for disease detection. In the late stage PM5, the best bands were different than the early stages, selected between 1005 nm and 1016 nm. This is in agreement with the result reported by Cao, Luo, Zhou, Duan, and Cheng (2013); they found that the most significant bands for PM detection in winter wheat was in the NIR range, while the reflectance in the visible range could not be used to detect the disease severity. For the very late stage PM6, the best bands were selected in blue range at 388–398 nm (Table 3). It can be observed from the best (most significant) bands selection, that in order to accurately differentiate between healthy and diseased plants, each PM stage needs to be monitored separately by focusing in different spectral ranges. The leaves with initial infection looked like healthy leaves, while the leaves in intermediate and late stage had white powder present on them and turned necrotic. As expected, the detection in the asymptomatic stage was the most challenging, due to the limited changes in the physiology and phenology of the plants at the first disease development stages. Khan et al. (2020) reported that in PM-infected wheat plants, the pigment concentration and photosynthetic ability were altered slightly at the early infection stage, but reduced quickly with the intensification of the disease severity. They found that the most significant bands capable for detecting PM in early infection stages were the near infrared bands. Zhang et al. (2012) confirmed that the chlorophyll content, pigment concentration and subsequent change in the carotenoids, anthocyanins and xanthophylls pigments were reduced during progress of PM in winter wheat.

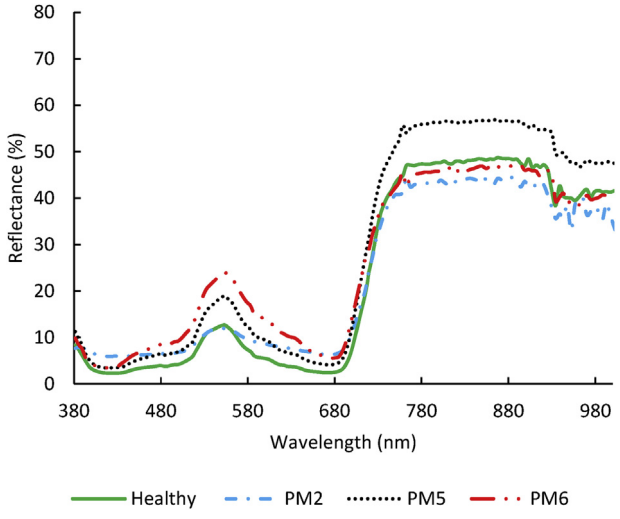

Fig. 6 – UAV-based spectral reflectance signatures of healthy squash plants and PM-infected plants in different disease development stages (asymptomatic, early and late stages).

3.2. *Spectral reflectance and classification analysis of PM-infected squash in field conditions (UAV-based)*

The UAV-based spectral reflectance of the squash plants was collected every 6–7 days, as the disease progressed in PM2, PM5, and PM6 stages (Table 1). It can be noticed that there is a significant difference between the spectral signatures of the different PM stages when compared to a healthy plant (Fig. 6). The spectral reflectance value increased in blue (400 nm), green (520–550 nm), red and red edge for all disease stages. It is important to note that there was a significant difference between spectral signatures of healthy and asymptomatic stage (PM2). The results were similar to the results of the

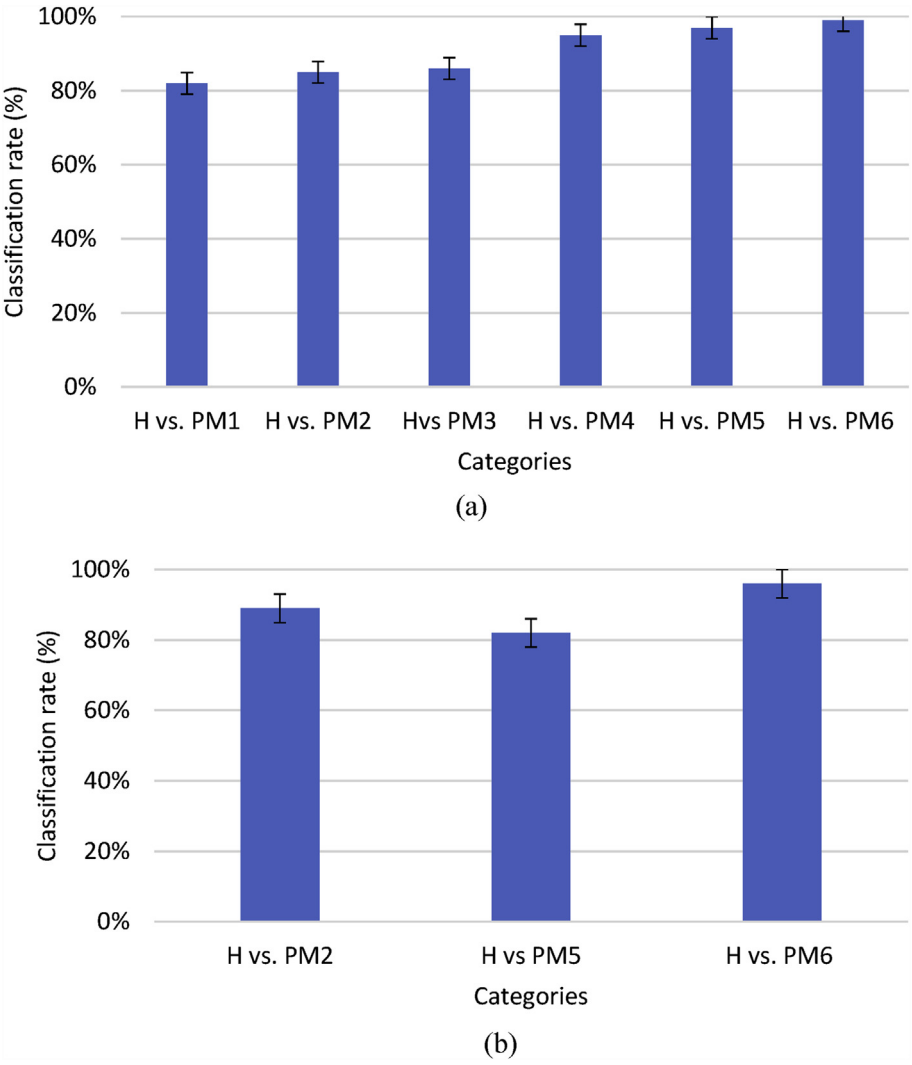

Fig. 8 – Classification results and standard error of using the RBF method for distinguishing healthy and PM-infected squash plants in different disease development stages in: a) laboratory, and b) field conditions (UAV-based).

Table 3 – The best (most significant) wavebands selected in laboratory and field conditions based on disease severity; the weight value of each band is reported in parenthesis. The Tukey's HSD test ($\alpha = 0.01$) was used; all weight values in the Table belong to the same group ("a").

Parameters category	Significant wavelength (nm)
Lab-based	
Healthy vs. PM1	991(100%), 976 (100%), 978 (99%), 992 (99%), 989 (98%)
Healthy vs. PM2	960 (100%), 964 (98%), 975 (98%), 966 (97%), 966 (97%)
Healthy vs PM3	975 (100), 964 (98%), 975 (98%), 966 (97%), 966 (97%)
Healthy vs. PM4	975 (100), 964 (98%), 975 (98%), 966 (97%), 966 (97%)
Healthy vs. PM5	1012 (100), 1014(99%), 1016 (98%), 1007 (98%), 1005 (97%)
Healthy vs. PM6	388 (100), 397 (99%), 394 (96%), 396 (94%), 390 (94%)
Field-based (UAV)	
Healthy vs. PM2	646 (100%), 650 (100%), 655 (99%), 656 (99%)
Healthy vs PM5	591 (100%), 583 (99%), 579 (99%)
Healthy vs. PM6	689 (100), 655 (98%), 659 (99%), 646 (98%)

laboratory measurements; the behavior of the spectral reflectance for field and laboratory measurements had the same structure especially in visible range. However, in NIR the spectral signature for both measurements had different spectral reflectance, especially for PM2 in the field. The PM2 had lower reflectance than in PM5 and PM6, while it was the opposite in NIR. Sensitivity values (Fig. 7) had peaks for PM2 and PM6 in blue and red range, which means that these spectral ranges could be used to differentiate these two disease stages.

The RBF classification of healthy vs. PM2 was 89% (Fig. 8b), hence, RBF was able to detect PM2 even with very few symptoms seen in the field. For healthy vs. PM5 the classification rate was lower when compared to the PM2, because of some external environmental conditions such as cloudy weather and due to some leaves in the field that weren't dry totally from previous rain. Kaufman and Remer (1994) suggested that the smoke dark clouds, dense vegetation and hazy atmospheres would affect remote sensing reflectance measurement. The highest classification value achieved was in very late disease stage PM6 at 96% (Fig. 8b). The most significant bands for differentiating between healthy and early stage were selected in red range at 646 nm, 655 nm, 591 nm, 689 nm (Table 3). In the red range, the spectral signature curve and sensitivity values recorded significant variances. In a healthy plant, most of the light is absorbed in blue and red range while reflecting light in the green range; so, any changes that might occur in the leaves could affect the light absorption in all ranges. This principle is used effectively in remote sensing, so the increase or decrease of spectral reflectance values in red range acts as an indicator for abnormal stress factors that could affect the spectral reflectance (Lu, Ehsani, Shi, de Castro, & Wang, 2018; Lu et al., 2017; Mahlein et al., 2013).

In the future, UAVs can be used to monitor different stages of a disease, differentiating between healthy, asymptomatic, and late stages. This disease development monitoring can help growers with determining the optimal timing and selection of fungicides that need to be applied based on the severity of the disease. This can effectively help in reducing the amount of chemicals and controlling the disease before it spreads to plants throughout the field or to neighboring plantings. An infected leaf begins to lose chlorophyll slowly, which turns it to yellow color. This affects the spectral reflectance in visible range. Mahlein et al. (2013) detected several diseases like PM, Cercospora leaf spot, and sugar beet rust in sugar beet crop by comparing spectral reflectance vales in the laboratory. These values were varied in visible and in NIR based on the disease development stage. Water content is very important for spectral reflectance analysis too. For example, after 2 weeks from the initial infection of a disease, leaves lose moisture content, making easier to differentiate between healthy and late stage diseased plants. One other factor that could affect the spectral reflectance is the increase of brown pigment content in the leaves (Penuelas & Filella, 1998). After few days from infection, fungal pathogens (like PM) can cover the entire surface of leaves and prevent the stomata and chlorophyll process to work properly; that would lead to damage in the leaf's tissue which ultimately results in dead leaf cells in few days (Daub & Ehrenshaft, 2000). The most challenging point to identify PM was that the disease begins in the lower canopy of the plants on the older leaves which are typically covered by the younger leaves higher in the canopy, so any infection of older leaves was difficult to be identified in very early stages. A low-to-ground sensing could help mitigate this issue. There are additional challenges when it comes to automatic disease detection (Barbedo, 2016), because there are multiple diseases or other stress factors with similar symptoms that would affect the spectral reflectance values, which makes it difficult to accurately identify a particular disease (Polder, van der Heijden, van Doorn, & Baltissen, 2014; Pourreza, Lee, Etxeberria, & Banerjee, 2015).

3.3. Most significant VIs for detecting PM development stages

3.3.1. Laboratory-based analysis

If the value of M value is more than 1.0, it presents a high and good discrimination ability (de Castro, Ehsani, Ploetz, Crane, & Abdulridha, 2015). The VIs with the highest M value in early stages (PM1 and PM2) were the water index (WI) and the photochemical reflectance index (PRI). However, M value trends were different in the advance stages PM3 to PM6. Figure 9a and b presents the VIs that would best distinguish between healthy and non-healthy plants. The VIs discrimination ability was varied based on the disease severity stages. In late stages of PM3, PM4, PM5 and PM6, WI was the VI with the highest discrimination ability for intermediate and very late stages of disease development. ARI and CVI were the VIs with lower discrimination ability in the early stage, while RVSI, TCARI, and RASAb were the VIs with lower discrimination ability in intermediate and late stages. In fact, leaves looked similar in the asymptomatic stage PM1 and early stage PM2, and it was very difficult to differentiate between them visually. In later stages, leaves had reduced chlorophyll concentration and the fungus covered the entire surface of the leaves preventing gas exchange, which led to reduced water content, which made the leaves look like they had drought symptoms (Pugliese, Gullino, & Garibaldi, 2010). The WI was utilised to evaluate the performance of hyperspectral reflectance to measure leaf water content (Kovar et al., 2019).

3.3.2. Field (UAV) based analysis

In field conditions, VIs were noticed to have their highest M values in the late disease development stages (PM6). Powdery mildew was detected from the UAV data even in very early stage (PM1&2), when the plants had green leaves and looked healthy (prior to visible symptoms). The trends of VIs in asymptomatic stage was unique from intermediate and late stage. For example, the Cl green, ND 750/705, GNDVI, SR 850 have the highest M values in late stage (PM6). The variation of the VIs trends in each stage is evidence that the spectral reflectance values were affected by changes in leaf properties such as chlorophyll content, water stress, cells damage, temperature of the canopy. All these factors will affect the spectral reflectance due to light being defused, transmitted or absorbed based on the leaf situation. The leaves of squash plants in asymptomatic stage have less water stress; the water or cell sap usually absorbs the light rather than reflects it. It was possible to detect PM even in asymptomatic stages by using the Cl green, ND 750/705, GNDVI, SR 850 (Fig. 10). Furthermore, it was possible to trace the disease development stages by using UAV collected data and specific VIs.

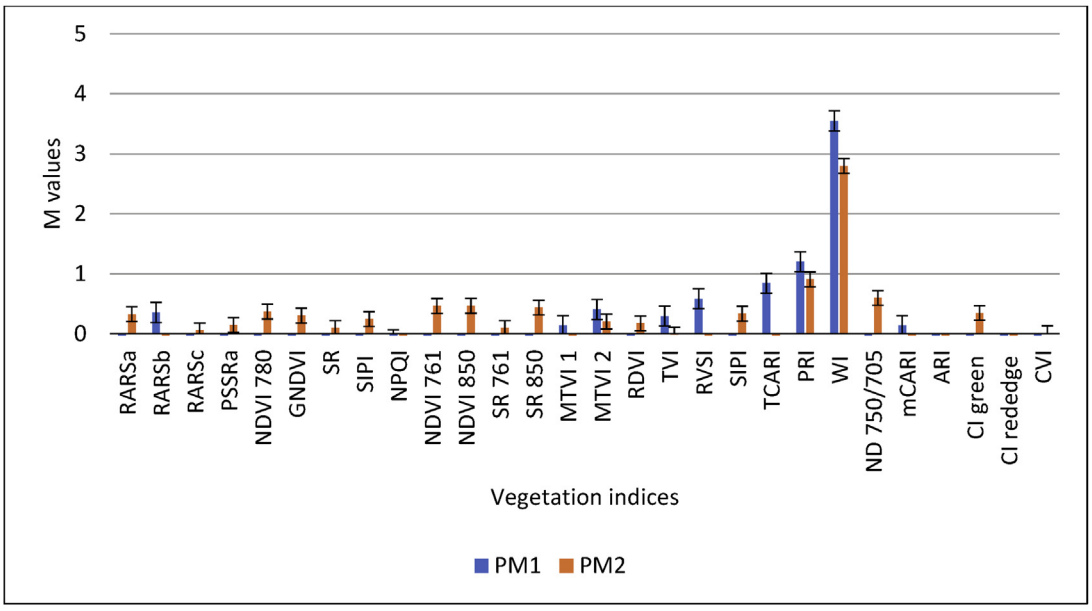

(a)

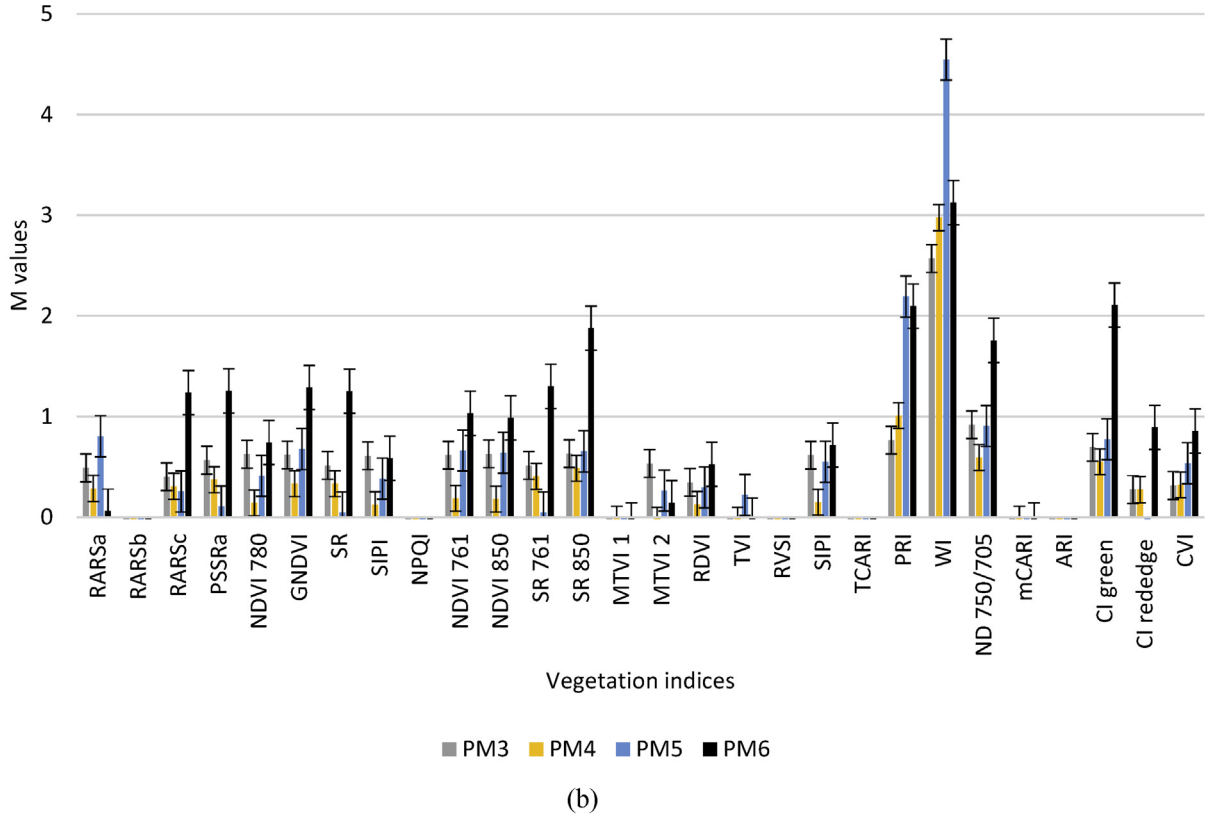

(b)

Fig. 9 – M values and standard errors for each VI in laboratory conditions for: a) PM1 and PM2 (early disease development stages); and b) PM3, PM4, PM5 and PM6 stages.

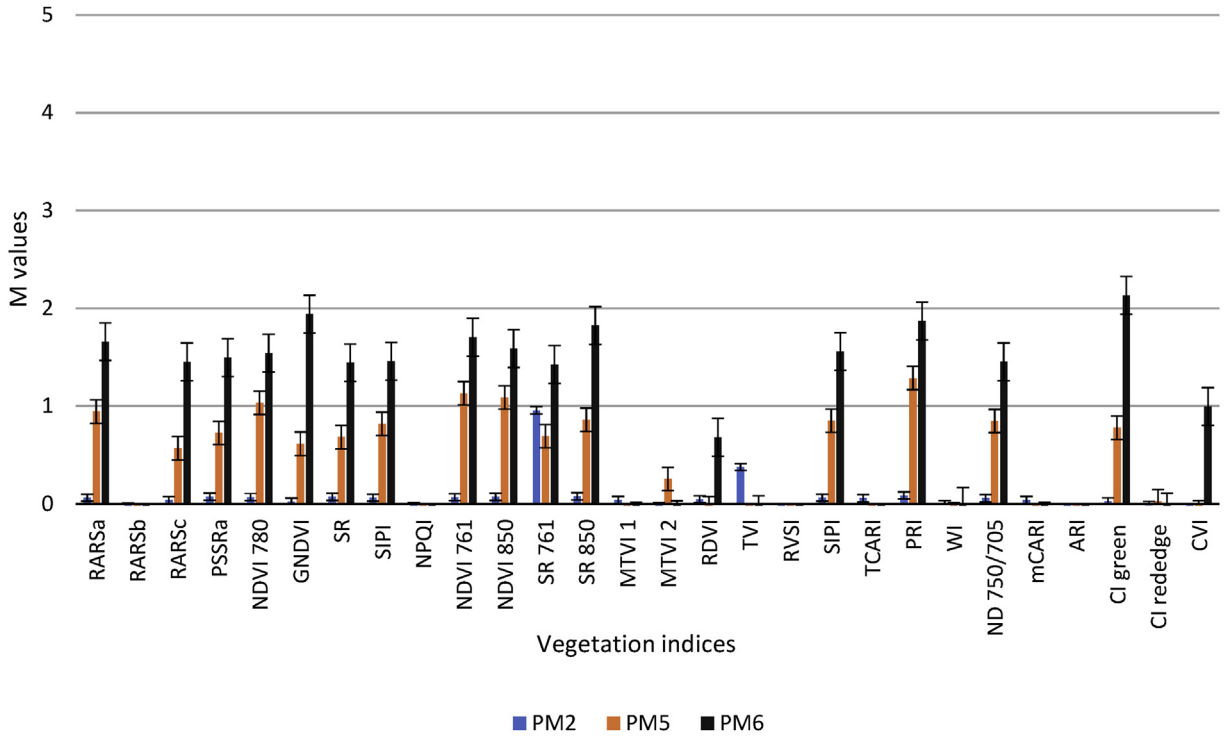

Fig. 10 – M values for each VI in field conditions (UAV-based) for PM2, PM5 and PM6.

4. Conclusion

Spectral reflectance analysis of squash leaves was performed in both laboratory and field conditions. The purpose of this study was to detect different disease development stages (asymptomatic, early, intermediate, and late disease) of PM. The best (most significant) bands were selected to differentiate between healthy plants and each of the disease development stages of PM-infected plants. Using the RBF method, the PM disease was detected even in the asymptomatic stages and under both laboratory and field conditions, with classification accuracies of 82% and 89% for the asymptomatic and early stage, respectively. The highest classification rate was obtained in the very late stage of the disease development at 96% and 99% for laboratory and field conditions, respectively. The most significant VIs that could differentiate between different PM stages were the water index (WI) in asymptomatic stage for laboratory conditions, and the Cl green, ND 750/705, GNDVI, SR 850 in early and late stages for laboratory and field (UAV-based) conditions. Hence, a low-cost UAV-based multispectral system can be developed to calculate the proposed VIs that can accurately distinguish between healthy and PM-infected squash plants. An additional study is needed to evaluate the detection accuracy of the proposed technique in mixed infection conditions (e.g., plants infected by multiple diseases).

Declaration of competing interest

The authors declare that they have no known competing financial interests or personal relationships that could have appeared to influence the work reported in this paper.

Acknowledgement

This material was made possible, in part, by a Cooperative Agreement from the U.S. Department of Agriculture's Agricultural Marketing Service through grant AM190100XXXXG036. Its contents are solely the responsibility of the authors and do not necessarily represent the official views of the USDA.

REFERENCES

Abdulridha, J., Ampatzidis, Y., Kakarla, S. C., & Roberts, P. (2019a). Detection of target spot and bacterial spot disease in tomato using UAV-based and benchtop-based hyperspectral imaging techniques. *Precision Agriculture*, 1–24.

Abdulridha, J., Batuman, O., & Ampatzidis, Y. (2019b). UAV-based remote sensing technique to detect citrus canker disease utilizing hyperspectral imaging and machine learning. *Remote Sensing, 11*(11), 1373.

Abdulridha, J., Ehsani, R., Abd-Elrahman, A., & Ampatzidis, Y. (2019c). A remote sensing technique for detecting laurel wilt disease in avocado in presence of other biotic and abiotic stresses. *Computers and Electronics in Agriculture, 156*, 549–557.

Abdulridha, J., Ehsani, R., & de Castro, A. (2016). Detection and differentiation between laurel wilt disease, Phytopthora disease and salinity damage using a hyperspectral sensing technique Agriculture. *Baseline, 6*(4), 56.

Al-Ahmadi, A. H., Subedi, A., Wang, G. X., Choudhary, R., Fakhoury, A., & Watson, D. G. (2018). Detection of charcoal rot (*Macrophomina phaseolina*) toxin effects in soybean (Glycine max) seedlings using hyperspectral spectroscopy. *Computers and Electronics in Agriculture, 150*, 188–195.

Ampatzidis, Y., De Bellis, L., & Luvisi, A. (2017). iPathology: Robotic applications and management of plants and plant diseases. *Sustainability, 9*(6), 1010.

Ampatzidis, Y., & Partel, V. (2019). UAV-based high throughput phenotyping in citrus utilizing multispectral imaging and artificial intelligence. *Remote Sensing, 11*(4), 410. https://doi.org/10.3390/rs11040410.

Ampatzidis, Y., Partel, V., & Costa, L. (2020). Agroview: Cloud-based application to process, analyze and visualize UAV-collected data for precision agriculture applications utilizing artificial intelligence. *Computers and Electronics in Agriculture, 174*(July), 105157. https://doi.org/10.1016/j.compag.2020.105457.

Atanassova, S., Nikolov, P., Valchev, N., & Stoyka Yorgov, D. (2019). *Early detection of powder mildew (Podoshaera xanthii) on cucumber leaves based on visible and near-infrared spectroscopy* (Vol. 2075). AIP Conference Proceedings.

Barbedo, J. G. A. (2016). A review on the main challenges in automatic plant disease identification based on visible range images. *Biosystems Engineering, 144*, 52–60.

Barnes, J. D., Balaguer, L., Manrique, E., Elvira, S., & Davison, A. W. (1992). A reappraisal of the use of DMSO for the extraction and determination of chlorophylls-a and chlorophylls-b in lichens and higher-plants. *Environmental and Experimental Botany, 32*(2), 85–100.

Blackburn, G. A. (1998). Spectral indices for estimating photosynthetic pigment concentrations: A test using senescent tree leaves. *International Journal of Remote Sensing, 19*(4), 657–675.

Brisbois, B. W., Harris, L., & Spiegel, J. M. (2018). Political ecologies of global health: Pesticide exposure in southwestern Ecuador's banana industry. *Antipode, 50*(1), 61–81.

Broge, N. H., & Leblanc, E. (2001). Comparing prediction power and stability of broadband and hyperspectral vegetation indices for estimation of green leaf area index and canopy chlorophyll density. *Remote Sensing of Environment, 76*(2), 156–172.

Candiago, S., Remondino, F., De Giglio, M., Dubbini, M., & Gattelli, M. (2015). Evaluating multispectral images and vegetation indices for precision farming applications from UAV images. *Remote Sensing, 7*(4), 4026–4047.

Cao, X., Luo, Y., Zhou, Y., Duan, X., & Cheng, D. (2013). Detection of powdery mildew in two winter wheat cultivars using canopy hyperspectral reflectance. *Crop Protection, 45*, 124–131.

Chappelle, E. W., Kim, M. S., & McMurtrey, J. E. (1992). Ration analysis of reflectance spectra (RARS)-An algorithm for the remote estimation concentration of chlorophyll-a, chlorophyll-b, and carotenoid soybean leaves. *Remote Sensing of Environment, 39*(3), 239–247.

Cohen, R., Hanan, A., & Paris, H. S. (2003). Single-gene resistance to powdery mildew in zucchini squash (Cucurbita pepo). *Euphytica, 130*(3), 433–441.

Couture, J. J., Singh, A., Charkowski, A. O., Groves, R. L., Gray, S. M., Bethke, P. C., & Townsend, P. A. (2018). Integrating spectroscopy with potato disease management. *Plant Disease, 102*(11), 2233–2240.

Daub, M. E., & Ehrenshaft, M. (2000). The photoactivated Cercospora toxin cercosporin: Contributions to plant disease and fundamental biology. *Annual Review of Phytopathology, 38*, 461.

de Castro, A. I., Ehsani, R., Ploetz, R., Crane, J. H., & Abdulridha, J. (2015). Optimum spectral and geometric parameters for early detection of laurel wilt disease in avocado. *Remote Sensing of Environment, 171*, 33–44.

Delnavaz, M., & Zangooei, H. (2016). Evaluation of moving bed biofilm reactor (MBBR) by applying adaptive neuro-fuzzy inference system (ANFIS), radial basis function (RBF) and Fuzzy Regression Analysis. *Iranian Journal of Environmental Technology, 2*(1), 27–40.

Faical, B. S., Freitas, H., Gomes, P. H., Mano, L. Y., Pessin, G., de Carvalho, A., & Ueyama, J. (2017). An adaptive approach for UAV-based pesticide spraying in dynamic environments. *Computers and Electronics in Agriculture, 138*, 210–223.

Gamon, J. A., Penuelas, J., & Field, C. B. (1992). A narrow-waveband spectral index that tracks diurnal changes in photosynthetic efficiency. *Remote Sensing of Environment, 41*(1), 35–44.

Gitelson, A. A., Gritz, Y., & Merzlyak, M. N. (2003). Relationships between leaf chlorophyll content and spectral reflectance and algorithms for non-destructive chlorophyll assessment in higher plant leaves. *Journal of Plant Physiology, 160*(3), 271–282.

Gitelson, A. A., & Merzlyak, M. N. (1996). Signature analysis of leaf reflectance spectra: Algorithm development for remote sensing of chlorophyll. *Journal of Plant Physiology, 148*(3–4), 494–500.

Gitelson, A. A., Merzlyak, M. N., & Chivkunova, O. B. (2001). Optical properties and nondestructive estimation of anthocyanin content in plant leaves. *Photochemistry and Photobiology, 74*(1), 38–45.

Haboudane, D., Miller, J. R., Pattey, E., Zarco-Tejada, P. J., & Strachan, I. B. (2004). Hyperspectral vegetation indices and novel algorithms for predicting green LAI of crop canopies: Modeling and validation in the context of precision agriculture. *Remote Sensing of Environment, 90*(3), 337–352.

Haboudane, D., Miller, J. R., Tremblay, N., Zarco-Tejada, P. J., & Dextraze, L. (2002). Integrated narrow-band vegetation indices for prediction of crop chlorophyll content for application to precision agriculture. *Remote Sensing of Environment, 81*(2–3), 416–426.

Hariharan, J., Fuller, J., Ampatzidis, Y., Abdulridha, J., & Lerwill, A. (2019). *Finite difference analysis and bivariate correlation of hyperspectral data for detecting laurel wilt disease and nutritional deficiency in avocado* (Vol. 11, p. 1748). Multidisciplinary Digital Publishing Institute.

Itoh, K. (2014). Study of the ecology of pesticide-degrading microorganisms in soil and an assessment of pesticide effects on the ecosystem. *Journal of Pesticide Science, 39*(3–4), 174–176.

Johansen, K., Morton, M. J. L., Malbeteau, Y. M., Aragon, B., Al-Mashharawi, S. K., Ziliani, M. G., & McCabe, M. F. (2019). Unmanned aerial vehicle-based phenotyping using morphometric and spectral analysis can quantify responses of wild tomato plants to salinity stress. *Frontiers of Plant Science, 10*.

Jordan, C.,F. (1969). Derivation of leaf area index from quality of light on the forest floor. *Ecology journal, 50*, 663–666.

Kaufman, Y. J., & Remer, L. A. (1994). Detection of forests using mid-ir reflectance-an application for aerosol studies. *IEEE Transactions on Geoscience and Remote Sensing, 32*(3), 672–683.

Khan, I., Haider, Liu, H., Cheng, T., Tian, Y., Chao Cao, Q., Yao, X., et al. (2020). Detection of wheat powdery mildew based on hyperspectral reflectance through SPA and PLS-LDA. *Int J Precis Agric Aviat, 3*(1), 13–22.

Kovar, M., Brestic, M., Sytar, O., Barek, V., Hauptvogel, P., & Zivcak, M. (2019). Evaluation of hyperspectral reflectance parameters to assess the leaf water content in soybean. *Water, 11*(3).

Lapushkina, E. E., Andreeva, A. M., & Slynko, Y. V. (2002). Features of the early development and and an analysis of resistance to the effects of pesticides in the bream Abramis brama (L.), the roach Rutilus rutilus (L.) and their first generation hybrids. In *Biology of inland waters: Problems of ecology and biodiversity: Materials of the twelfth international conference of young scientists* (pp. 23–26). Papanina: Institut Biologii Vnutrennikh Vod im. ID. September 2002.

Lu, J. Z., Ehsani, R., Shi, Y. Y., Abdulridha, J., de Castro, A. I., & Xu, Y. J. (2017). Field detection of anthracnose crown rot in strawberry using spectroscopy technology. *Computers and Electronics in Agriculture, 135*, 289–299.

Lu, J. Z., Ehsani, R., Shi, Y. Y., de Castro, A. I., & Wang, S. (2018). Detection of multi-tomato leaf diseases (late blight, target and

bacterial spots) in different stages by using a spectral-based sensor. *Scientific Reports, 8*.
Luvisi, A., Ampatzidis, Y. G., & De Bellis, L. (2016). Plant pathology and information technology: Opportunity for management of disease outbreak and applications in regulation frameworks. *Sustainability, 8*(8).
Mahlein, A. K., Rumpf, T., Welke, P., Dehne, H. W., Pluemer, L., Steiner, U., & Oerke, E. C. (2013). Development of spectral indices for detecting and identifying plant diseases. *Remote Sensing of Environment, 128*, 21–30.
Martinelli, F., Scalenghe, R., Davino, S., Panno, S., Scuderi, G., Ruisi, P., & Dandekar, A. M. (2015). Advanced methods of plant disease detection. *A review. Agronomy for Sustainable Development, 35*(1), 1–25.
McGrath, M.,T. (1997). *Powdery mildew of cucumber*. Retrieved from New York State-Cornell University. Fact Sheet Page: 732.30. Last update 2017 http://vegetablemdonline.ppath.cornell.edu/factsheets/Cucurbits_PM.htm.
McGrath, M.,T., Fox, G.,M., & Menasha, S. (2009). *Powdery mildew resistant zucchini squash variety evaluation, New York*.
Merton, R. (1998). Monitoring community hysteresis using spectral shift analysis and the red-edge vegetation stress index. In *JPL airborne earth science workshop*. Pasadena, California, USA: NASA, Jet Propulsion Laboratory.
Partel, V., Kakarla, C., & Ampatzidis, Y. (2019). Development and evaluation of a low-cost and smart technology for precision weed management utilising artificial intelligence. *Computers and Electronics in Agriculture, 157*, 339–350.
Penuelas, J., Baret, F., & Filella, I. (1995). Semiempirical indexes to assess carotenoids chlorophyll-a ratio from leaf spectral reflectance. *Photosynthetica, 31*(2), 221–230.
Penuelas, J., & Filella, I. (1998). Visible and near-infrared reflectance techniques for diagnosing plant physiological status. *Trends in Plant Science, 3*(4), 151–156.
Penuelas, J., Llusia, J., Pinol, J., & Filella, I. (1997a). Photochemical reflectance index and leaf photosynthetic radiation-use-efficiency assessment in Mediterranean trees. *International Journal of Remote Sensing, 18*(13), 2863–2868.
Penuelas, J., Pinol, J., Ogaya, R., & Filella, I. (1997b). Estimation of plant water concentration by the reflectance water index WI (R900/R970). *International Journal of Remote Sensing, 18*(13), 2869–2875.
Polder, G., van der Heijden, G., van Doorn, J., & Baltissen, T. (2014). Automatic detection of tulip breaking virus (TBV) in tulip fields using machine vision. *Biosystems Engineering, 117*, 35–42.
Pourreza, A., Lee, W. S., Etxeberria, E., & Banerjee, A. (2015). An evaluation of a vision-based sensor performance in Huanglongbing disease identification. *Biosystems Engineering, 130*, 13–22.
Pugliese, M., Gullino, M. L., & Garibaldi, A. (2010). Effects of elevated CO2 and temperature on interactions of grapevine and powdery mildew: First results under phytotron conditions. *Journal of Plant Diseases and Protection, 117*(1), 9–14.
Raun, W. R., Solie, J. B., Johnson, G. V., Stone, M. L., Lukina, E. V., Thomas, W. E., & Schepers, J. S. (2001). In-season prediction of potential grain yield in winter wheat using canopy reflectance. *Agronomy Journal, 93*(1), 131–138.
Reuveni, R.,J. (1974). *Effect of humidity on epidemiological patterns of the powdery mildew* (Sphaerotheca fuliginea) *on squash*. Phytoparasitica.
Roujean, J. L., & Breon, F. M. (1995). Estimating par absorbed by vegetation from bidirectional reflectance measurements. *Remote Sensing of Environment, 51*(3), 375–384.
Semeraro, T., Mastroleo, G., Pomes, A., Luvisi, A., Gissi, E., & Aretano, R. (2019). Modelling fuzzy combination of remote sensing vegetation index for durum wheat crop analysis. *Computers and Electronics in Agriculture, 156*, 684–692.
Spurgeon, D., Hesketh, H., Lahive, E., Svendsen, C., Baas, J., Robinson, A., & Heard, M. (2016). Chronic oral lethal and sub-lethal toxicities of different binary mixtures of pesticides and contaminants in bees (Apis mellifera, Osmia bicornis and Bombus terrestris) center for ecology & hydrology. *EFSA Supporting Publications, 13*(9), EN–1076.
Tripodi, P., Massa, D., Venezia, A., & Cardi, T. (2018). Sensing technologies for precision phenotyping in vegetable crops: Current status and future challenges. *Agronomy-Basel, 8*(4).
Vincini, M., Frazzi, E., & D'Alessio, P. (2007). Comparison of narrow-band and broad-band vegetation indexes for canopy chlorophyll density estimation in sugar beet. In J. V. Stafford (Ed.), *Precision agriculture '07: Proceedings of the 6th European conference on precision agriculture* (pp. 189–196). Wageningen, The Netherlands: Wageningen Academic Publishers.
Xiongkui, H., Aijun, Z., Liu, & Jianli, S. (2011). Precision orchard sprayer based on automatically infrared target detecting and electrostatic spraying techniques. *International Journal of Agricultural and Biological Engineering, 4*(1), 35.
Xu, H. R., Ying, Y. B., Fu, X. P., & Zhu, S. P. (2007). Near-infrared spectroscopy in detecting leaf minor damage on tomato leaf. *Biosystems Engineering, 96*(4), 447–454.
Zhang, J. C., Pu, R. L., Wang, J. H., Huang, W. J., Yuan, L., & Luo, J. H. (2012). Detecting powdery mildew of winter wheat using leaf level hyperspectral measurements. *Computers and Electronics in Agriculture, 85*, 13–23.
Zheng, Q., Huang, W. J., Cui, X. M., Dong, Y. Y., Shi, Y., Ma, H. Q., et al. (2019). Identification of wheat yellow rust using optimal three-band spectral indices in different growth stages. *Sensors, 19*(1).